Article

Cancer Cell

Targeting the AAA ATPase p97 as an Approach to Treat Cancer through Disruption of Protein Homeostasis

Highlights

- CB-5083 is a potent and selective small-molecule inhibitor of the cancer target p97
- CB-5083 induced a strong unfolded protein response leading to cancer cell death
- CB-5083 has antitumor effects in vivo in multiple myeloma and solid tumor models

Authors

Daniel J. Anderson, Ronan Le Moigne, Stevan Djakovic, ..., Han-Jie Zhou, David Wustrow, Mark Rolfe

Correspondence

danderson@cleavebio.com

In Brief

Anderson et al. characterize CB-5083 as a potent, selective, and orally bioavailable inhibitor of p97, a AAA-ATPase critical for regulating protein homeostasis pathways. CB-5083 activates the apoptotic arm of the unfolded protein response and has antitumor activity in several hematological and solid tumor models.

Accession Numbers

GSE73588

Anderson et al., 2015, Cancer Cell *28*, 653–665
November 9, 2015
http://dx.doi.org/10.1016/j.ccell.2015.10.002

CellPress

Cancer Cell
Article

CellPress

Targeting the AAA ATPase p97 as an Approach to Treat Cancer through Disruption of Protein Homeostasis

Daniel J. Anderson,[1,*] Ronan Le Moigne,[1] Stevan Djakovic,[1] Brajesh Kumar,[1] Julie Rice,[1] Steve Wong,[1] Jinhai Wang,[1] Bing Yao,[1] Eduardo Valle,[1] Szerenke Kiss von Soly,[1] Antonett Madriaga,[1] Ferdie Soriano,[1] Mary-Kamala Menon,[1] Zhi Yong Wu,[1] Martin Kampmann,[2] Yuwen Chen,[2] Jonathan S. Weissman,[2] Blake T. Aftab,[3] F. Michael Yakes,[1] Laura Shawver,[1] Han-Jie Zhou,[1] David Wustrow,[1] and Mark Rolfe[1]
[1]Cleave Biosciences, Inc., Burlingame, CA 94010, USA
[2]Department of Cellular and Molecular Pharmacology and Howard Hughes Medical Institute
[3]Division of Hematology & Oncology, Department of Medicine, Helen Diller Family Cancer Center
University of California, San Francisco, San Francisco, CA 94158, USA
*Correspondence: danderson@cleavebio.com
http://dx.doi.org/10.1016/j.ccell.2015.10.002

SUMMARY

p97 is a AAA-ATPase with multiple cellular functions, one of which is critical regulation of protein homeostasis pathways. We describe the characterization of CB-5083, a potent, selective, and orally bioavailable inhibitor of p97. Treatment of tumor cells with CB-5083 leads to accumulation of poly-ubiquitinated proteins, retention of endoplasmic reticulum-associated degradation (ERAD) substrates, and generation of irresolvable proteotoxic stress, leading to activation of the apoptotic arm of the unfolded protein response. In xenograft models, CB-5083 causes modulation of key p97-related pathways, induces apoptosis, and has antitumor activity in a broad range of both hematological and solid tumor models. Molecular determinants of CB-5083 activity include expression of genes in the ERAD pathway, providing a potential strategy for patient selection.

INTRODUCTION

Oncogene-targeted therapies have made important contributions to the treatment of cancer (Ramos and Bentires-Alj, 2014), but resistance to these therapies is common and likely to be a consequence of the plasticity and heterogeneity of cancer cell populations (Meacham and Morrison, 2013). The concept of non-oncogene addiction has recently been used to describe cellular processes that are not intrinsically oncogenic but on which certain cancer cells rely for accelerated and unregulated growth (Luo et al., 2009). These non-oncogene addiction pathways include DNA damage repair, mitosis, metabolism, immune response, epigenetics, and protein homeostasis. By targeting these pathways, the aim is to mitigate cancer cell growth even when diverse oncogenic mutations are at play.

"Protein homeostasis" refers to the balance among protein synthesis, folding, quality control, and degradation and encompasses various pathways that many cancer cells are heavily reliant upon for their growth and survival. The high protein synthetic rate and rapid cell cycle of these cancer cells can make them more dependent on the "quality control" provided by the ubiquitin proteasome system (UPS), a central pathway controlling the degradative aspect of protein homeostasis (Van Drie, 2011). The relevance of targeting the UPS has been proven in the clinical setting by the success of the proteasome inhibitors in hematologic malignancies (Wustrow et al., 2013). However, development of resistance (Ruschak et al., 2011) and lack of activity in solid tumor settings (Milano et al., 2009; Wright, 2010) support the need to develop inhibitors of other regulators of protein homeostasis.

Significance

Protein homeostasis pathways have become attractive targets for treatment of certain tumor types because of the high protein synthetic rate of these tumors and their consequent heightened dependence on degradative pathways for their growth and survival. p97 is a key mediator of several protein homeostasis processes and is therefore a strong potential cancer target. We identified a small-molecule compound, CB-5083, that blocks p97 activity through ATP-competitive binding and has physicochemical properties that enable oral administration. CB-5083 exhibited antitumor activity in tumor models in which proteasome inhibitors were inactive. We characterized molecular determinants of sensitivity so that clinical development can be focused on tumor subsets more likely to show a response.

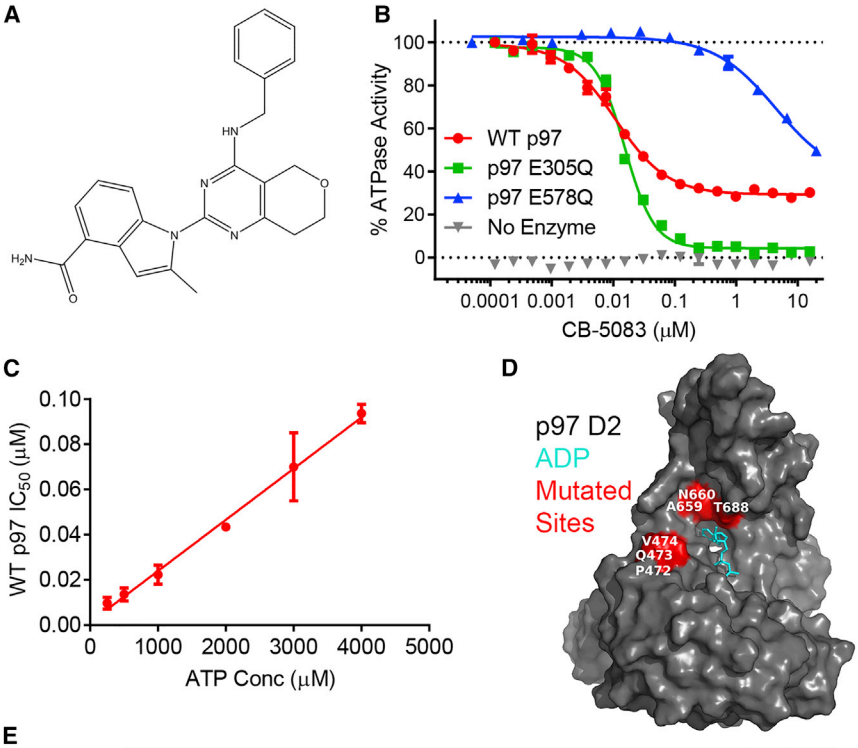

E

	p97 Biochem			A549 Viability		
	mean IC_{50} (μM)	Stdev	n	mean EC_{50} (μM)	Stdev	n
ML-240	0.329	0.256	11	3.34	0.52	6
NMS-873	0.069	0.017	7	2.68	0.08	5
CB-5083	0.011	0.004	18	0.67	0.16	43

Figure 1. CB-5083 Is a Potent Inhibitor of p97's D2 ATPase Domain

(A) Chemical structure of CB-5083.

(B) Dose-response curve of CB-5083 with recombinant WT p97, p97E305Q, and p97E578Q mutant proteins in an NADH coupled ATPase assay. The assay was conducted at 60 nM enzyme, 500 μM ATP, and shown concentrations of CB-5083. R^2 values were 0.98, 0.99, and 0.97 for WT, E305Q, and E578Q, respectively.

(C) ATP competition assay of CB-5083 with WT p97 with increasing ATP concentration.

(D) Crystal structure of p97-D2 showing ADP binding site and relative position of mutations found in resistant cells.

(E) Comparison of IC_{50} values of shown compounds for p97 in biochemical assay using NADH-based ATPase assay and cell viability assays using ADP-glo.

Error bars are ±SEM. See also Figure S1 and Tables S1 and S2.

p97, also known as Valosin-containing protein, is an essential and conserved member of the AAA family of adenosine triphosphatases (ATPases). Although the cellular functions associated with p97 are diverse, including organelle membrane homotypic fusion and sorting of endosomal cargo, it is clear that one of its most important functions is as a key regulator of protein homeostasis (Meyer et al., 2012). Through interaction with a number of distinct cofactors, p97 mediates the extraction of proteins destined for destruction by the UPS from organelles, chromatin, and protein complexes. For example, interaction with UBX cofactors mediates interactions with various E3 ligases to direct p97 to certain protein degradation processes. p97 is a key regulator of endoplasmic reticulum (ER)-associated degradation (ERAD), which is the main quality control mechanism for soluble, membrane-associated, glycosylated proteins as well as non-glycosylated proteins as they are processed through the ER (Rabinovich et al., 2002; Ye et al., 2001). The unfolded protein response (UPR) is a pathway that acts both to resolve unfolded protein stress and to trigger cell death when the buildup of such unfolded proteins becomes irresolvable (Miura, 2014). Given that many cancer cells can have a high reliance on their UPR and ERAD pathways as a result of their high protein synthetic burden and possibly aneuploidy (Deshaies, 2014; Oromendia and Amon, 2014), and that a block in ERAD following inhibition of p97 function is likely to lead to irresolvable proteotoxic stress, these pathways provide a potential targetable vulnerability in cancer cells.

Recent efforts to discover small-molecule inhibitors of p97 have resulted in the identification of several classes of well-characterized ATP-competitive and allosteric inhibitors (Chou et al., 2011, 2013; Magnaghi et al., 2013). Although these compounds have served as important tools to understand more fully the cellular consequences of inhibiting p97, they have modest potency, their specificity is not fully characterized, and they lack the drug-like properties required for in vivo pre-clinical and clinical development. We set out to discover a potent and specific small-molecule inhibitor of p97 with drug-like properties to allow the clinical evaluation of targeting this important component of protein homeostasis as a therapeutic approach to treat cancer.

RESULTS

CB-5083 Is a Potent and Selective Inhibitor of p97

DBeQ and ML240 (Chou et al., 2011, 2013) were used as starting points to initiate extensive lead optimization efforts that led to the identification of the compound CB-5083 with improved p97 inhibition in biochemical and cellular assays along with pharmaceutical properties suitable for clinical development (unpublished data). CB-5083 (1-[4-(benzylamino)-5H,7H,8H-pyrano [4,3-d]pyrimidin-2-yl]-2-methyl-1H-indole-4-carboxamide) is a p97 ATPase activity inhibitor with a biochemical half maximal inhibitory concentration (IC_{50}) of 11 nM when tested at an ATP concentration of 500 μM (Figures 1A, 1B, and S1A). Addition of high concentrations of ATP to the biochemical assay caused an increase in the IC_{50} of CB-5083, indicating competitive inhibition of at least one of the two ATP binding sites in p97 (Figure 1C). The first p97 AAA-ATPase domain (D1), which has a minor contribution to overall ATPase activity, is situated near the amino-terminal domain that interacts with various cofactors. The second AAA-ATPase domain (D2) is the main driver of ATPase activity in

biochemical reactions (Song et al., 2003). An ATP hydrolysis-deficient mutant of the D1 ATPase site (E305Q) was inhibited by CB-5083 at a similar potency as wild-type (WT) p97 with an IC_{50} of 15.4 nM, whereas we were unable to calculate an IC_{50} for the D2 ATP hydrolysis mutant (E578Q) because of limitations in solubility above 20 μM, suggesting high selectivity of CB-5083 for the D2 ATPase site of p97 (Figures 1B and S1B) (Dalal et al., 2004). Interestingly, in an ATPase biochemical assay that contains an ATP regeneration system, the maximum inhibition of WT p97 was only 70.7%, whereas in an ATPase assay without an ATP regeneration system, maximum inhibition was 95.6%, suggesting that in the presence of ADP, the contribution to ATP hydrolysis of the D1 ATPase site is minimal but in the CB-5083 D2-bound state with low ADP concentrations the ATP hydrolysis of D1 is substantial (Figure S1C). Therefore, CB-5083 is characterized as a D2-selective and potent inhibitor (Figure 1E).

In order to determine the selectivity of CB-5083 for the D2 domain of p97 over other ATP-using enzymes, a probe binding/mass spectrometry approach was used (Patricelli et al., 2011). When tumor cell lysates were incubated with the biotinylated ATP probe and 10 μM CB-5083, mass spectrometry was used to identify which peptides were no longer bound by the probe in the presence of CB-5083. The D2 ATPase site of p97 was not bound by the probe in the presence of CB-5083, whereas the D1 ATPase site of p97 was still efficiently bound, further confirming the D2 selectivity and ATP competitive binding of CB-5083 (Figure S1D). Among the 164 ATPase sites and 194 kinase sites bound by the probe in the tumor cell lysate, only DNA-PK, mTOR, and PIK3C3 were identified to have significant reduction of binding with 10 μM CB-5083 treatment (Figure S1D; Table S1). Consistent with this finding, when CB-5083 was tested in a panel of kinase biochemical assays at a dose of 5 μM, DNA-PK, mTOR, and PIK3C3 were the top hits. Subsequent dose titration assays revealed that CB-5083 had 29.6-, 128-, and 158-fold less affinity for DNA-PK, mTOR, and PIK3C3, respectively, compared with p97 (Figures S1D and S1E and Table S2). Furthermore, in a cell-based assay, CB-5083 was shown not to inhibit DNA-PK at concentrations that caused cell death (Figure S1F). Together these data suggest that CB-5083 is a highly selective inhibitor for the D2 site of p97.

Generating drug-adapted cell lines that harbor resistance followed by target gene sequencing is a method that can be used to determine compound specificity (Wacker et al., 2012). To identify the cellular target of CB-5083, HCT116 colon cancer cells were treated with increasing concentrations of CB-5083, and mutation-driven, drug-resistant clones were selected. Resistant clones demonstrated 2- to 50-fold shifts in the half maximal growth inhibition of CB-5083 in a 72 hr viability assay (Figure S1G). p97 cDNA was isolated from these clones and sequenced. Single homozygous coding mutations that mapped either directly in or adjacent to the D2 ATPase domain were found in the majority of CB-5083-resistant clones (Figures 1D and S1H). Furthermore, when several of the identified mutations were introduced into recombinant p97, changes in biochemical potency of CB-5083 were similar to what was seen in mutant cell viability. The mutant cell viability and recombinant protein sensitivity results suggest that p97 mutations are driving cellular resistance in the analyzed clones, further supporting on-target specificity of CB-5083 (Figures S1I and S1J).

Cellular Effects of CB-5083

We next wanted to characterize the cellular pharmacodynamic (PD) effects of CB-5083. Given the prominent role of p97 in ERAD, we treated human embryonic kidney 293T cells stably expressing TCRα-GFP, a validated ERAD substrate (DeLaBarre et al., 2006), with CB-5083. CB-5083 treatment led to a dose-dependent accumulation of TCRα-GFP in the ER with a half maximal effective concentration (EC_{50}) of 0.73 ± 0.04 μM, suggesting a direct block in ER extraction (Figures 2A and 2B). On the contrary, inhibition of proteasome activity with bortezomib led to an accumulation of TCRα-GFP in the cytoplasm and aggresomes, suggesting that blocking protein degradation is not sufficient to trap TCRα-GFP in the ER. To determine if CB-5083 blocks ERAD-independent protein degradation, we evaluated the stability of the cytoplasmic UPS substrate GFPu (Bence et al., 2001). The accumulation of GFPu was observed after CB-5083 treatment with similar potency to what was seen with TCRα-GFP (EC_{50} = 1.05 ± 0.01 μM) (Figures S2A and S2B). To monitor the impact on endogenous substrate degradation, we measured accumulation of endogenous K48 poly-ubiquitinated proteins visualized by immunofluorescence in the lung carcinoma cell line A549. Accumulation of poly-ubiquitinated proteins following CB-5083 treatment was seen initially in the cytoplasm but then primarily in the nucleus at later time points, supporting the notion that ERAD-independent substrate degradation is also blocked (Figures 2C, 2D, and S2C). The predominant nuclear accumulation of K48 poly-ubiquitin with CB-5083 was in contrast to bortezomib treatment that caused poly-ubiquitinated protein accumulation primarily in the cytoplasm and aggresomes (Figures 2C, 2D, and S2D). Consistent with a p97 role in nuclear protein extraction (Meerang et al., 2011), A549 cells transfected with small interfering RNA (siRNA) oligonucleotides targeting p97 that led to a reduction in p97 protein levels showed a similar nuclear accumulation of K48 poly-ubiquitin compared with CB-5083 treatment (Figures S2E and S2F). Additionally, K48-ubiquitinated proteins from CB-5083-treated HCT116 cells accumulated at a higher molecular weight compared with bortezomib-treated cells (Figure 2E). These data suggest that p97 inhibition has a direct role in nuclear and cytosolic protein degradation in addition to its effect on ERAD.

p97 has also been shown to play a critical role in autophagy, another major cellular pathway for protein degradation (Bug and Meyer, 2012). To determine if CB-5083 modulated autophagy, we visualized the autophagy adaptor protein p62 (also known as sequestosome 1) (Bjørkøy et al., 2006) by immunofluorescence after drug treatment in A549 cells (Figures 2C, 2F, and S2C). Upon CB-5083 treatment, p62 was targeted to peri-nuclear foci, some of which co-localized with the K48 poly-ubiquitin and microtubule-associated protein 1A/1B-light chain 3 (LC3) puncta. These foci rapidly cleared from cells, a phenotype that is consistent with the activation of autophagy, which is in contradiction to the previously defined role for p97 as a mediator of autophagy. In support of the notion that CB-5083 activates rather than inhibits autophagy, the mTOR inhibitor INK-128, which activates autophagy (Schenone et al., 2011), also caused a decrease in p62 levels (Figures 2F and S2G). Conversely, the autophagy inhibitor bafilomycin A1 (Yamamoto et al., 1998) caused an accumulation of p62 in peri-nuclear foci that co-localized with the key autophagy regulator LC3. Additionally,

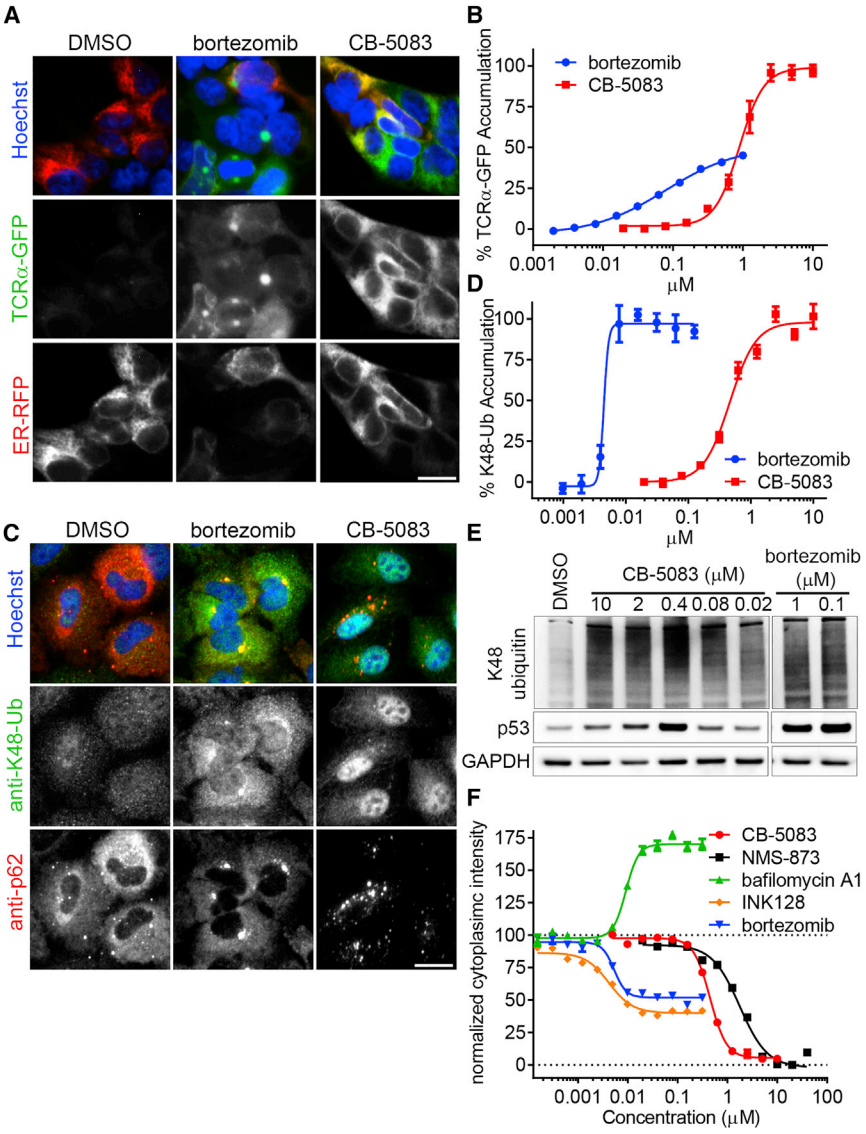

Figure 2. CB-5083 Blocks Major Cellular Protein Degradation Functions

(A) Example images of human embryonic kidney 293 (HEK293) cells expressing TCRα-GFP with RFP labeled ER (ER-RFP) treated with 2.5 μM CB-5083 or 1 μM bortezomib for 6 hr. The scale bar represents 20 μm and applies to all images.

(B) Analysis of TCRα-GFP fluorescence in cells treated with dose titration of CB-5083 or bortezomib. R^2 values were 0.95 and 0.93 for bortezomib and CB-5083, respectively.

(C) Example images of non-small-cell lung cancer cell line A549 labeled with anti-K48-ubiquitin (K48-Ub) and anti-p62 antibodies treated with 2.5 μM CB-5083 or 1 μM bortezomib for 6 hr. The scale bar represents 20 μm and applies to all images.

(D) K48-Ub and p62 were evaluated by immunofluorescence in A549 cells treated with dose titration of CB-5083 or bortezomib. R^2 values were 0.91 and 0.94 for bortezomib and CB-5083, respectively.

(E) Colon cancer cell line HCT116 was treated with CB-5083 or bortezomib for 24 hr. K48-Ub conjugates and p53 were analyzed by western blot.

(F) p62 modulation was evaluated by immunofluorescence in A549 cells treated with CB-5083, bortezomib, NMS-873, INK128, and bafilomycin A1. R^2 values were and 0.96, 0.93, 0.83, 0.78, and 0.86 for CB-5083, NMS-873, bafilomycin A1, INK128, and bortezomib, respectively.

Error bars are ±SEM. See also Figure S2.

bortezomib, which had previously been shown to induce autophagy, and NMS-873, a structurally distinct p97 inhibitor, both caused decreases in p62 levels. siRNA-mediated knockdown of p97 also caused a punctate redistribution and a decrease in the level of p62, suggesting that the observed CB-5083 effect on this pathway is through p97 (Figures S2H). To determine if the loss of p62 was mediated through autophagy, CB-5083 was combined with bafilomycin A1, this resulted in a block of the p62 clearance seen with CB-5083 alone (Figure S2I). These data indicate that autophagy is likely activated by CB-5083, which is consistent with studies that report induction of ER stress leads to strong autophagy activation (Ogata et al., 2006).

Accumulation of misfolded proteins in the ER and other organelles can trigger the UPR (Sano and Reed, 2013). The UPR can be activated via one of three pathways: inositol-requiring enzyme 1, activating transcription factor 6 (ATF6), or protein kinase R-like kinase (PERK). CB-5083 caused activation of all three branches of the UPR to levels that were greater in most cases than treatment with bortezomib and comparable with treatment with the sarcoplasmic ER calcium-ATPase inhibitor thapsigargin or the glycosylation inhibitor tunicamycin (Figures 3A and 3B). Induction of any branch of the UPR can lead to the accumulation of the transcription factor CCAAT/enhancer-binding protein homologous protein (CHOP) (Wang et al., 2007; Yoshida et al., 2000). A rapid and sustained induction of CHOP protein was seen with CB-5083 treatment of A549 cells, with an EC_{50} of 1.19 ± 0.23 μM (Figures 3A, 3C, S3A, and S3B).

To further investigate UPR activation, the expression levels of genes involved in UPR and ER function were measured by RT-PCR after cells were treated with CB-5083. Many genes were upregulated upon CB-5083 treatment (Figure 3D; Table S3). *CHOP* was the most highly upregulated gene within the RT-PCR panel in both A549 cells and colorectal carcinoma cell line HCT116 when treated with CB-5083. Heat shock 70 kDa protein 5 (BiP), which is an ER-resident chaperone involved directly in the UPR, and other genes less directly involved were also upregulated, suggesting a strong transcriptional response of this pathway (Table S3). Genes encoding several components of the ERAD machinery, such as *HERPUD1*, *SEL1L*, *SYVN1*, *EDEM1*, and *HSPA5*, were also among the most upregulated genes, suggesting a potential compensatory mechanism specific to the inhibition of ERAD. To determine if CB-5083-mediated induction of gene expression was specific to the UPR, transcriptome expression analysis was conducted using RNA

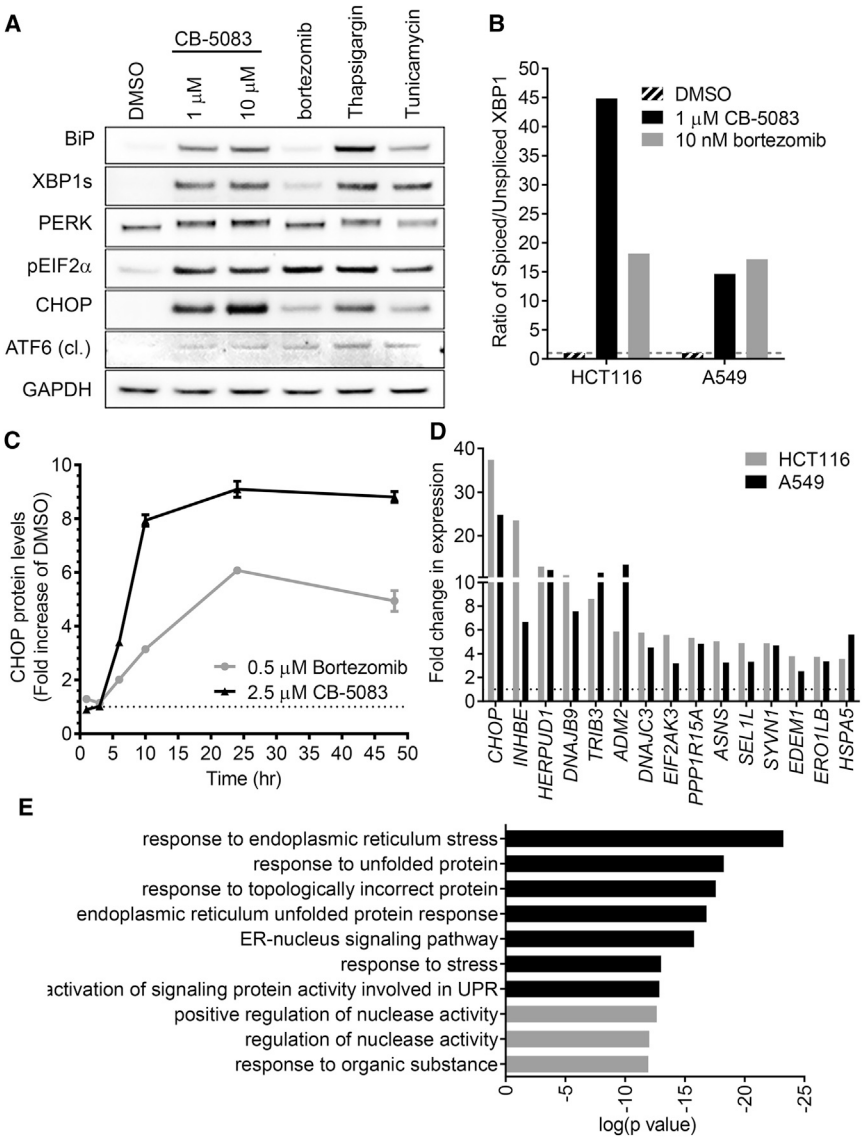

Figure 3. CB-5083 Induces a Strong UPR

(A) A549 cells were treated with CB-5083, bortezomib (1 μM), thapsigargin (1 μM), or tunicamycin (2 μg/ml) for 8 hr. Western blot analysis was performed with antibodies against BiP, spliced XBP1 (XBP1s), PERK, phospho-EIF2a, CHOP, cleaved (cl) ATF6, and GAPDH.

(B) A549 or HCT116 cells were treated with CB-5083 (1 μM) or bortezomib (10 nM) for 8 hr. Relative gene expression of spliced and unspliced XBP1 were measured by RT-PCR.

(C) A549 cells were treated with CB-5083 (2.5 μM) or bortezomib (0.5 μM) for the indicated times, and CHOP protein levels were quantified by immunofluorescence staining.

(D) A549 or HCT116 cells were treated with CB-5083 (1 μM) for 8 hr. Relative gene expression of a panel of UPR genes, spliced XBP1, and unspliced XBP1 were measured by RT-PCR.

(E) HCT116 cells were treated with CB-5083 (1 μM) for 8 hr and processed for RNA-seq. GO enrichment analysis was performed on top 500 upregulated genes. The top ten most significant GO terms are listed.

Error bars are ±SEM. See also Figure S3 and Table S3.

sequencing (RNA-seq). Following gene ontology (GO) enrichment analysis of upregulated genes, we found that the most significant GO terms were related to UPR or ER stress (Figure 3E). Together, these data suggest that CB-5083 causes a strong and specific UPR response in cancer cells, which is very consistent with a specific inhibition of its target, p97.

CB-5083 Causes Cancer Cell Death

Death receptor 5 (DR5) has recently been shown to play an essential role in UPR-induced cell death (Lu et al., 2014). Consistent with induction of the UPR, CB-5083 induced an 18.9-fold upregulation of DR5 mRNA and a 7.7-fold upregulation of DR5 protein in HCT116 cells after 24 hr of treatment (Figures 4A and S4A), and increases in DR5 protein were seen at time points when increases in CHOP were observed (Figures S4A and S4B). DR5 has been shown to activate caspase-8 as a means of initiating the apoptosis cascade (Lu et al., 2014). Upon CB-5083 treatment in A549 and HCT116 cells, induction of caspase-8 and caspase-3/7 coincided with upregulation of DR5 (Figures 4B and 4C). Viability in both of these cell lines also began to decrease with a timing that was coincident with DR5 induction and caspase activation (Figure 4D). Potencies of cell death were similar to potencies of K48 poly-ubiquitin and CHOP protein accumulation, suggesting that the buildup of proteins marked for degradation and induction of the UPR may be linked to cell death (Figures 2D, S3B, and S4C).

To determine if CHOP pathway induction was driving cellular cytotoxicity, HCT116 cells were treated with CB-5083 after siRNA-mediated knockdown of BiP, PERK, CHOP, DR5, or caspase-8 (Figure 4E). Knockdown of BiP, which is a chaperone protein that acts in protective mechanisms of the UPR (Morris et al., 1997), did not block the decrease in viability seen with CB-5083 treatment. siRNA-mediated knockdown of CHOP, but not PERK, blocked CB-5083-mediated cell death, suggesting that not all UPR pathways mediate CB-5083-induced cell death. Knockdown of DR5 and caspase-8, which act downstream of CHOP to mediate apoptosis, also caused a block in CB-5083-induced cell death. Similar effects were seen in A549 cells when DR5 and caspase-8 were knocked down (Figure S4D). Furthermore, when cells were treated with siRNA oligos targeting DR5, DR5 protein induction upon CB-5083 treatment was strongly reduced (Figure S4A). When CB-5083 was combined with the CDK inhibitor dinaciclib, which inhibits the induction of CHOP (Nguyen and Grant, 2014), antagonism of cellular cytotoxicity was observed (Figure S4E). Together these data strongly support the conclusion that CHOP-mediated apoptosis

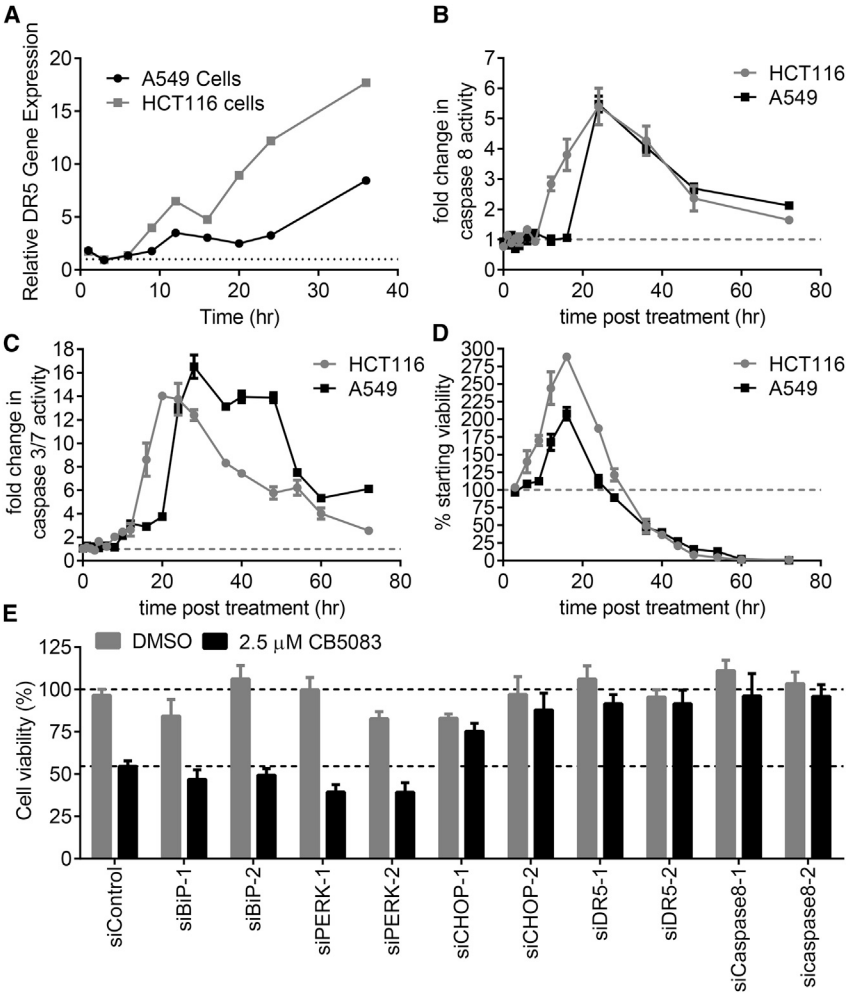

Figure 4. Induction of UPR by CB-5083 Causes Cancer Cell Death

(A) A549 cells were treated with CB-5083 (1 μM) for the indicated times. Relative DR5 gene expression was measured by RT-PCR.

(B–D) A549 or HCT116 cells were treated with CB-5083 (5 μM) for up to 72 hr. Caspase-8 activity (B), caspase-3/7 activity (C), and cell count (D) were measured at indicated times.

(E) BiP, PERK, CHOP, DR5, and caspase-8 were knocked down in HCT116 cells for 24 hr. Cells were then treated with CB-5083 (2.5 μM) for 24 hr, and cell viability was measured by cell titer glo.

Error bars are ±SEM. See also Figure S4.

is an important mechanism of CB-5083-induced cellular cytotoxicity.

CB-5083 Induces the UPR and Apoptosis in Xenograft Tumor Models

To evaluate its pharmacokinetic (PK) and PD activity, CB-5083 was administered at escalating dose levels to female nude mice bearing HCT116 xenograft tumors. Following a single oral dose of CB-5083, there was a dose-dependent increase in area under the plasma concentration versus time curve (Figure 5A). Accumulation of poly-ubiquitin and CHOP in tumor tissue was observed in a dose-dependent manner (Figures 5B and 5C). Increases in DR5 protein were also seen (Figure S5A). Additionally, p62 protein levels decreased by 60% at 6 hr at the 100 mg/kg dose level, consistent with what was observed in vitro (Figure 5D). To determine if markers of apoptosis were activated in CB-5083-treated xenograft models, the levels of cleaved poly ADP ribose polymerase (PARP) were monitored. Increases in cleaved PARP were observed in a dose-dependent manner with timing that was consistent with the induction of CHOP (Figure 5E). These data demonstrate that CB-5083 achieved plasma concentrations that were sufficient to elicit a PD as well as an apoptotic response in tumors.

CB-5083 Has Antitumor Activity in Xenograft Tumor Models

Given the strong UPR and apoptotic response seen with CB-5083 treatment in animal models, the antitumor activity of CB-5083 was assessed in nude or SCID-Beige mice bearing established human tumor xenografts derived from tumor cell lines of different histologic origins: HCT116 derived from colorectal adenocarcinoma, NCI-H1838 derived from non-small-cell lung cancer, AMO-1 derived from a plasmacytoma, and two colorectal cancer patient-derived xenograft (PDX) models (Figures 5F and 5G). CB-5083 was administered by oral gavage once (qd) or twice (bid) daily or following a 4 days on, 3 days off (qd4/3off) cycle. Inhibition of tumor growth (% TGI) was calculated on the last day of treatment. All CB-5083 dosing schedules tested were tolerated in tumor-bearing mice, generally resulting in weight loss of <10% (Figures S5B–S5D). The qd4/3off schedule offered the best therapeutic index, with significant (78%, $p < 0.0001$) TGI of HCT116 tumor observed at 100 mg/kg (Figure 5F). In contrast, a 25 mg/kg bid dose induced 54% TGI ($p < 0.0001$), and a 50 mg/kg qd dose resulted in 62% TGI ($p < 0.0001$). These results were consistent with the PK and PD results, where 100 mg/kg clearly induced the highest level of apoptosis after a single administration (Figures 5A–5E), and support the notion of dose-dependent antitumor activity. To confirm that the antitumor effects with CB-5083 in the HCT116 xenograft model were due to inhibition of p97, the resistant HCT116 cell line model harboring the T688A p97 mutation, which causes strong biochemical and cellular resistance to CB-5083, was tested. Tumor growth of this mutant model was not inhibited when dosed with CB-5083 at 90 mg/kg (Figure S5E). Strong antitumor activity was seen with the qd4/3off schedule in NCI-H1838 xenografts and the colorectal carcinoma PDX models. AMO-1 was the most sensitive cell line identified among 350 cell lines that were tested in vitro (IC_{50} = 81 nM; see below) and gave the most striking result in xenograft growth inhibition, with complete regressions of tumors observed in 6 of 12 animals after two cycles of treatment (Figure 5G). The activity seen in the AMO1

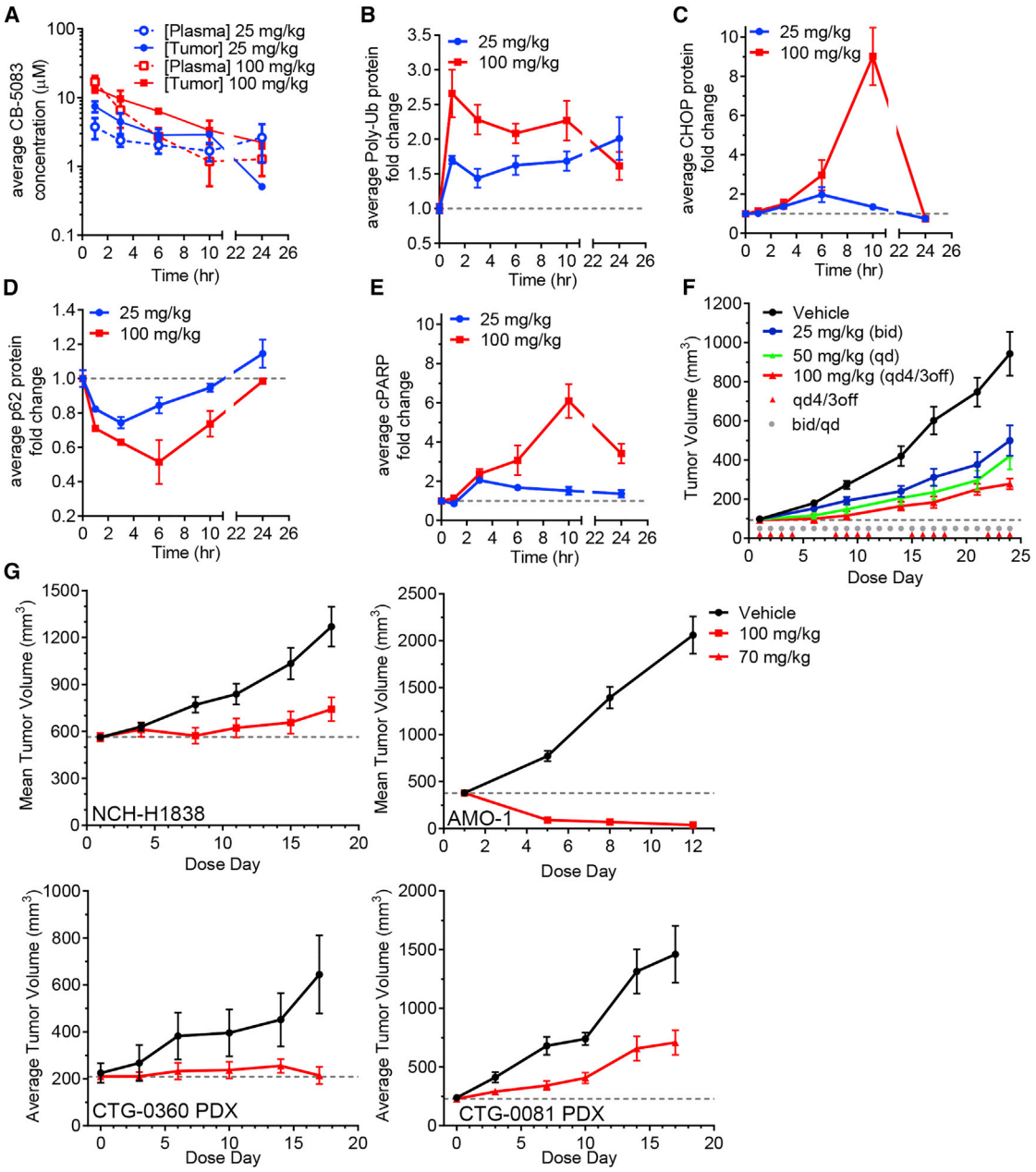

Figure 5. CB-5083 Has Activity in Mouse Models

(A) Tumor (open box) and plasma (open circle) concentrations of CB-5083 in tumor tissue extracts from nude mice bearing HCT116 tumors after treatment at 25 and 100 mg/kg.

(B–E) Levels of poly-ubiquitin (B), CHOP (C), p62 (D), and cleaved PARP (E) were measured in tumor tissue extracts from nude mice bearing HCT116 tumors after treatment at 25 and 100 mg/kg of CB-5083.

(F) Tumor growth was measured for various CB-5083 dosing schedules in the HCT116 xenograft model (n = 7–10).

(G) Tumor growth was measured with dosing of CB-5083 in NCI-H1838 (n = 16), AMO-1 (n = 12), CTG-0360 (n = 4), and CTG-0081 (n = 4) xenograft models. Error bars are ±SEM. See also Figure S5.

xenograft, a model derived from multiple myeloma, is consistent with the high sensitivity seen in this indication for other protein homeostasis pathway inhibitors such as bortezomib (Hideshima et al., 2001). These results demonstrate that oral treatment with CB-5083 inhibits the growth of human tumor xenografts in mice.

CB-5083 Is More Effective in Solid Tumor Models Than Proteasome Inhibitors

To understand further the antitumor effect of CB-5083 and the advantage of targeting protein homeostasis via inhibition of p97, comparative studies with proteasome inhibitors were conducted in solid tumor xenograft models. Proteasome inhibitors

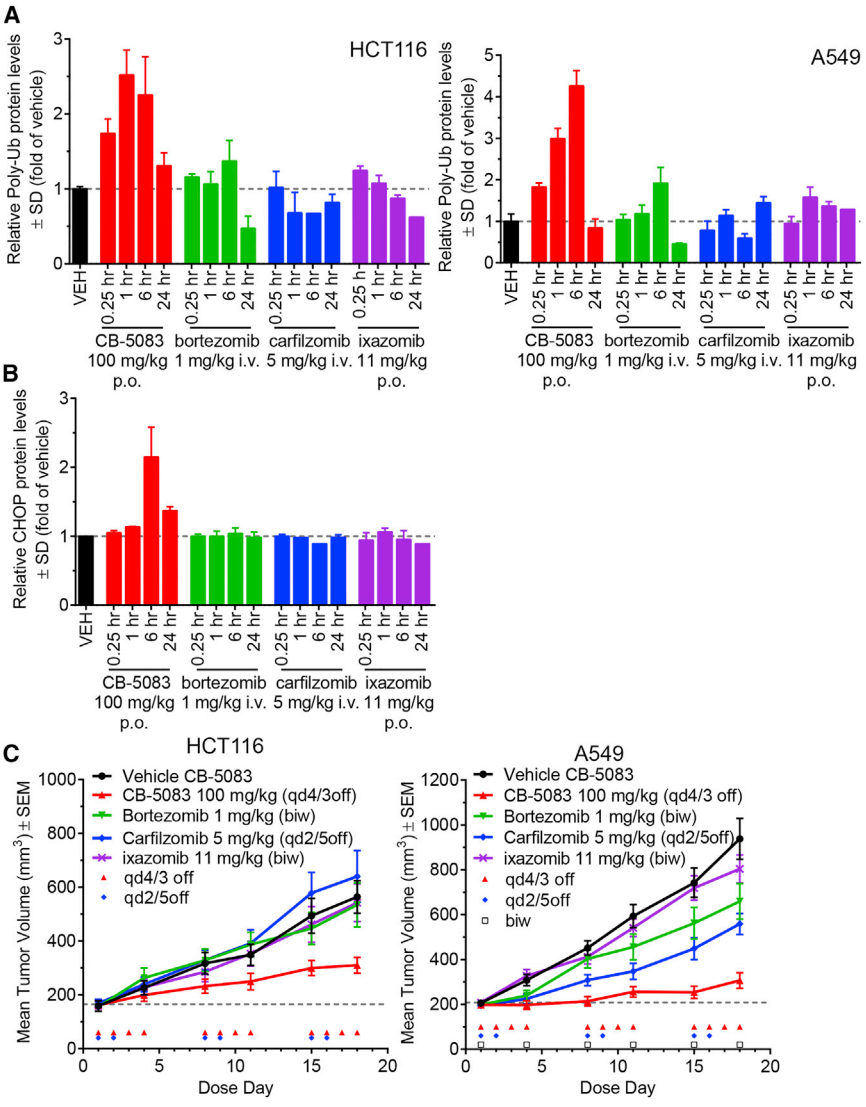

Figure 6. CB-5083 Demonstrates Greater Activity Than Proteasome Inhibitors in Solid Tumor Models

(A) Relative levels of poly-ubiquitin measured in HCT116 or A549 xenografts in mice administered CB-5083 or proteasome inhibitors (n = 3 per time point).

(B) Relative levels of CHOP measured in HCT116 xenografts in (A).

(C) Tumor growth was measured with dosing of CB-5083 or proteasome inhibitors in HCT116 (n = 8–12) and A549 (n = 10–12) xenograft models. Error bars are ±SEM. See also Figure S6.

are approved for the treatment of multiple myeloma (bortezomib and carfilzomib) and mantle cell lymphoma (bortezomib) but have failed to show sustainable activity in solid tumors (Milano et al., 2009; Wright, 2010). We compared the PD activity of CB-5083, bortezomib, carfilzomib, and ixazomib in female nude mice bearing HCT116 or A549 tumors. All agents were dosed at their optimal dosing route and published active dose in hematological models (Kupperman et al., 2010; Teicher et al., 1999; Zhang et al., 2013) and were generally well tolerated after repeat dosing (Figure S6). After a single administration of CB-5083, a strong and sustained induction of poly-ubiquitin was observed in tumor tissue, suggesting inhibition of the protein homeostasis pathway (Figure 6A). Additionally, a clear CHOP protein accumulation 6 hr after dosing was seen with CB-5083 (Figure 6B), suggesting UPR activation in these tumors. In contrast to CB-5083, none of the proteasome inhibitors were able to show significant, sustained accumulation of poly-ubiquitin or CHOP. The clear difference seen in the PD experiment was confirmed by evaluating tumor growth inhibition. CB-5083 showed a significant antitumor response in HCT116 xenografts (Figure 6C; TGI = 63%, $p < 0.0001$), whereas none of the proteasome inhibitors were active in this model. In A549 (Figure 6C), CB-5083 was the most potent agent, with 85% TGI ($p < 0.001$). In this model, carfilzomib (TGI = 50%, $p < 0.0001$) and bortezomib (TGI = 37%, $p < 0.0001$) showed modest activity, whereas ixazomib was inactive (TGI = 19%, $p = 0.0285$). Together these data demonstrate that targeting p97 may be a more effective strategy for inhibiting solid tumor growth than targeting the proteasome.

Determinants of CB-5083 Sensitivity

Given the variability in potency seen both in cell culture and in animals, we wanted to determine the molecular determinants of CB-5083 sensitivity or resistance. Potency of cell death induction was measured in 350 cancer cell lines representing a variety of tumor histologies (Figure 7A). The range in sensitivity to CB-5083 was narrow in this cell line panel, with EC_{50} values ranging from 81 nM to 2.1 μM, possibly owing to the pleiotropic cellular functions of p97. A good correlation was seen between EC_{50} and TGI for cell lines in which antitumor activity had been measured in vivo (R^2 = 0.51), suggesting that molecular determinants that drive sensitivity to CB-5083 may translate from cell culture to xenograft models (Figure 7B). Genomic data for the cell line panel were obtained from the Cancer Cell Line Encyclopedia (CCLE) (Barretina et al., 2012) and analyzed to determine which molecular and gene expression alterations correlated with CB-5083 sensitivity. Using linear regression, gene expression and copy number information from CCLE was compared with CB-5083 sensitivity. Ninety-three genes by mRNA expression and 94 gene loci by copy number were identified to correlate significantly with either CB-5083 sensitivity or resistance, as determined by the false discovery method (Benjamini and Yekutieli, 2001). To further validate the significance of gene correlates with CB-5083 sensitivity, drug sensitivity was randomized prior to linear regression,

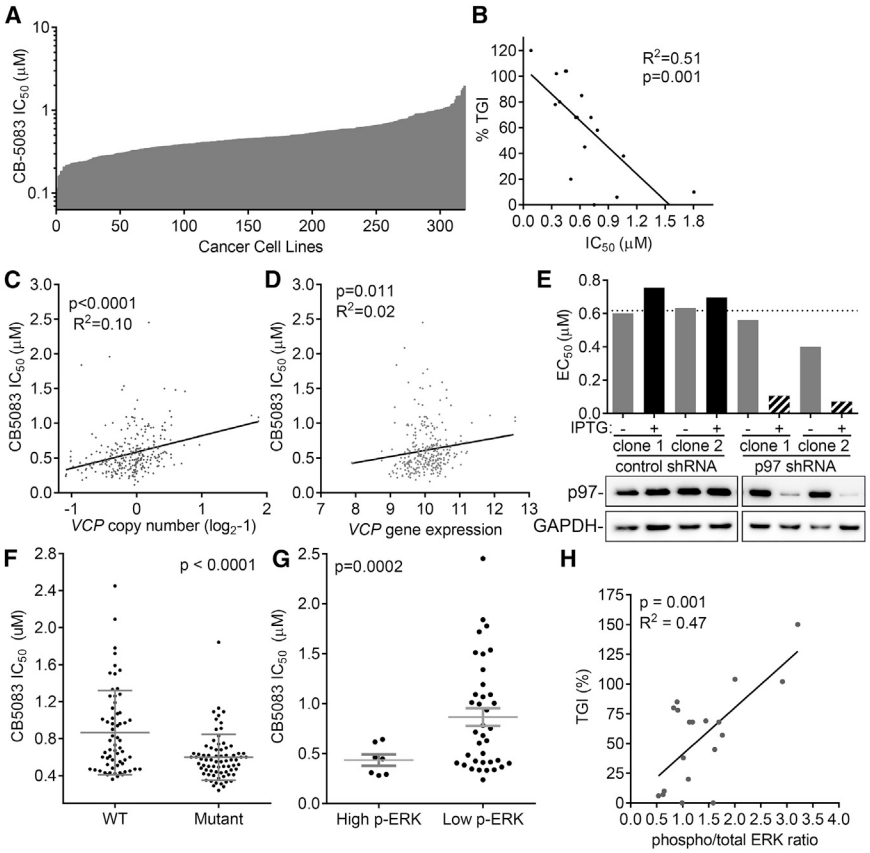

Figure 7. Activation of MAPK Pathway Correlates with Sensitivity to CB-5083 in Cancer Cells

(A) Three hundred forty cancer cell lines were treated with a dose titration of CB-5083, and EC_{50} of cell viability was measured at 72 hr. Cell lines are ordered by EC_{50}.

(B) TGI of a panel of cell lines in subcutaneous xenografts after oral administration of 100 mg/kg CB-5083 on a qd4/3off schedule for 3–4 weeks was compared with EC_{50} of the same cell lines grown in culture in a 72 hr viability assay.

(C) p97 gene copy number as measured by hybrid capture was plotted against CB-5083 EC_{50} of viability in a panel of cancer cell lines. Statistical significance of fit to linear regression was calculated with an F test (p value).

(D) p97 mRNA level as measured by microarray was plotted against CB-5083 EC_{50} of viability in a panel of cancer cell lines. Statistical significance of fit to linear regression was calculated with an F test (p value).

(E) Viability in A549 cells stably expressing inducible control shRNA or shRNA targeting p97 after 3 days of 500 μM IPTG treatment to induce the expression of shRNAs followed by 3 days of CB-5083 treatment. EC_{50} values were compared with p97 protein levels as measured by western blot.

(F) CB-5083 EC_{50} of viability in cell lines containing an oncogenic mutation in *KRAS*, *NRAS*, *HRAS*, *BRAF*, or *NF1* were compared with cells that were WT for all of these genes.

(G) CB-5083 EC_{50} values of viability in cell lines with high or low levels of phosphorylated ERK1 and ERK2 were compared.

(H) TGI for a set of cell lines grown as xenografts was plotted against the ratio of phosphorylated ERK1+ ERK2 to total ERK1+ ERK2 as measured by western blot.

See also Figure S7.

resulting in a strong decrease in the significance of the gene correlates, which further supports that the un-randomized gene correlates are biologically significant (Figure S7A).

Both gene copy number and mRNA level of p97 correlated with resistance to CB-5083 treatment with statistical significance, but given the low Pearson correlation (r) values, it is clear that other determinants of sensitivity exist across the diverse cell panel (Figures 7C and 7D). To determine if p97 levels specify sensitivity to CB-5083, we cloned individual p97-targeted single guide RNAs within the CRISPRi and CRISPRa platform in K562 leukemia cells (Gilbert et al., 2014) and quantified their effect on p97 expression by quantitative PCR (qPCR). Changes in the p97 mRNA level were moderate, likely because of the high basal expression of this abundant protein. We then determined the effect of p97 mRNA expression levels on CB-5083 sensitivity in a competitive growth assay and found an excellent correlation, with a Pearson correlation (R^2) of 0.97 (Figures S7B–S7D). Additionally, when p97 was knocked down in HCT116 cells using a stable inducible small hairpin RNA (shRNA) system resulting in a strong reduction in protein, CB-5083 EC_{50} shifted on average from 0.48 μM in the uninduced cells to 0.09 μM in the induced cells (Figures 7E and S7E–S7H). Together, the connection between p97 mRNA and protein expression and drug sensitivity further supports the notion of on-target antitumor activity of CB-5083.

High gene expression of DR5 was among the top correlates with CB-5083 sensitivity (Figure S7I), which is consistent with the UPR-cell death pathway being critical for CB-5083-mediated cell death. High expression of two genes involved in ERAD were also identified as correlating with CB-5083 sensitivity: autocrine motility factor receptor (AMFR/gp78), which is an E3 that directly associates with p97 (Song et al., 2005), and enhancing α-mannosidase-like protein (EDEM1), which recognizes misfolded proteins and is tethered to p97 through the Derlins (Oda et al., 2006) (Figure S7I). Together these data suggest that cells with elevated ERAD and UPR activity may be more susceptible to p97 inhibition.

When gene mutations were compared with CB-5083 sensitivity, *KRAS* and *BRAF* were among the top correlating mutant genes. Given the role of the mitogen-activated protein kinase (MAPK) pathway in stimulating protein synthesis (Dasgupta et al., 2005), activating mutations in this pathway may cause an increased dependency on the UPS. When cell lines with any mutation in genes associated with driving MAPK activation were compared with WT cells, there was also a correlation between activating mutations and sensitivity to CB-5083

(Figure 7F). To look at downstream activation of the MAPK pathway, phosphorylation of extracellular-signal-regulated kinases 1 and 2 (ERK1/2) was monitored. Samples with high levels of phospho-ERK1/2 were more sensitive to CB-5083, both in cell culture and xenograft models (Figures 7G, 7H, and S7L). Together these data suggest that cancer cells with activation of the MAPK pathway may rely heavily on p97's function in protein homeostasis and thus be more sensitive to an inhibitor of p97 such as CB-5083.

DISCUSSION

There is growing evidence that p97 is an important regulator of proteotoxic stress and protein homeostasis; thus, inhibition of p97 function provides an opportunity to target a key vulnerability of cancer (Deshaies, 2014). We have described the activity of a p97 small-molecule inhibitor with drug-like properties. CB-5083 is a potent p97 inhibitor that exhibits strong selectivity against other ATPases and kinases. Although no detectable inhibition of other ATPases and only minor inhibition of several kinases was observed, it remains possible that CB-5083 could target additional ATPases that may have not been captured by our mass spectrometry approach or biochemical screening. However, there is clear evidence that if this were the case, it does not contribute strongly to cellular cytotoxicity seen with CB-5083. When resistant mutant cell lines were generated against CB-5083, amino acid mutations within the D2 ATPase region of p97 were identified and recapitulated in recombinant protein, leading to 50-fold shifts in cell EC_{50}. Together these data give us confidence that the vast majority of cellular phenotypes and cytotoxicity induced by CB-5083 are driven through p97 inhibition.

Inhibition of p97 through CB-5083 was shown to have a profound effect on the UPR, activating all three arms of this conserved stress response pathway. It is intriguing that the extent of UPR activation induced by CB-5083 was markedly higher than that induced by the proteasome inhibitor bortezomib. Consistent with a recent study that characterized the sequential degradative pathway for a specific ERAD substrate (Morris et al., 2014), bortezomib treatment appeared to allow for the exit of TCRα from the ER, which may be the cause of lower UPR induction compared with p97 inhibition, where protein substrates are trapped in the ER following CB-5083 treatment. Alternatively, the differential induction of the UPR by CB-5083 and bortezomib may be due to the different subset of proteins whose degradation is blocked by these key regulators of protein homeostasis.

Our data suggest that the primary mechanism of cell death for CB-5083 appeared to be mediated through irresolvable proteotoxic stress. CHOP and DR5 induction caused by CB-5083 treatment was required for early induction of caspase activity and cellular cytotoxicity. At later time points, cells do eventually die with CHOP or DR5 depletion (data not shown), suggesting that there are other mechanisms of cellular cytotoxicity when p97 is inhibited or that knockdown is not complete. This is not surprising given the numerous cellular functions assigned to p97. Consistent with this notion, Eeyarestatin I, a p97-interacting molecule that also binds directly to ER membranes, induces cell death through ATF3, ATF4, and Noxa (Wang et al., 2009, 2010). These alternative routes of cell death observed may be due to the different mode of binding between CB-5083 and Eeyarestatin I or to different cellular systems used in these studies.

Interestingly, it appeared as though not all cellular functions of p97 were inhibited by CB-5083. For example, we did not see disruption of Golgi or ER morphology at active concentrations of CB-5083 (data not shown), suggesting that the membrane homotypic fusion function of p97 may not be blocked. Additionally, p97 has been widely reported to be required for the process of autophagy (Ju et al., 2009; Meyer et al., 2012). The marked clearance of p62 suggests that autophagy is not inhibited with CB-5083 treatment. Possibilities that could explain the lack of activity of CB-5083 on certain p97 functions are its specificity for the D2 ATPase domain of p97 or that it binds preferentially to a specific p97-containing cofactor complex. Recent work reported differential activity of p97 inhibitors on D1 and D2 sites as well as shifts in potency in the presence of the p47 cofactor (Fang et al., 2015). It will be interesting to interrogate the specific cofactor interactions of CB-5083-bound p97 and how these might relate to certain cellular functions. The role of autophagy as a compensatory mechanism to evade the effects of a p97 inhibitor remains unclear, although other approved anti-cancer agents appear to induce autophagy to a similar extent.

Several small-molecule inhibitors of p97 have been described in the literature (Chou et al., 2011, 2013; Magnaghi et al., 2013), but none has demonstrated in vivo activity. CB-5083 has demonstrated drug-like pharmaceutical properties and modulates UPS, UPR, and autophagy pathway markers in animal models with magnitudes and timings that are similar to what was seen in cell culture experiments, suggesting that inhibition of p97 leads to the same phenotypes in vivo as it does in vitro. CB-5083 also has strong antitumor activity in hematological and solid tumor models. CB-5083 was less active in HCT116 tumors harboring a resistant p97 point mutation, suggesting that the efficacy seen in other models is a result of on-target activity. The activity seen in solid tumor models treated with CB-5083 may have profound implications for targeting protein homeostasis beyond hematological disorders, which has been difficult to achieve in the clinic with proteasome inhibitors (Johnson, 2015). Higher UPR induction seen with p97 inhibition in vivo combined with oral administration allowing sustained exposure of drug in the plasma may also contribute to greater solid tumor activity compared with proteasome inhibitors and may provide an opportunity to identify patients more likely to respond to CB-5083 (see below).

Given the potential role of p97 in normal cells, it will be important to establish the molecular determinants of tumor cell sensitivity to CB-5083 in order to better identify patients that might have a clinical response at dose levels that are also well tolerated. By screening a large panel of cancer cell lines, we were able to identify statistically significant genomic features that correlate with either CB-5083 sensitivity or resistance. The identification of high p97 copy number and expression levels as genomic features that correlate with resistance to CB-5083 is intriguing. These data further validated p97 as the cellular target of CB-5083 and suggest that elevated levels of p97 may be a viable exclusion criterion in the clinic. However, p97 expression level has been reported to correlate with poor prognosis (Fessart

et al., 2013), suggesting that high expression of p97 may drive cancer progression. p97 appears to fall in the category of drug targets where expression of a target correlates with resistance to a given inhibitor, such as the classical example of DHFR amplification in methotrexate-resistant cells (Cillo et al., 1987), rather than correlating with sensitivity, such as was recently reported for the mitochondrial protein degradation enzyme ClpP (Cole et al., 2015).

The correlation of high expression of UPR- and ERAD-related genes with sensitivity to CB-5083 further supports the role of the UPR as the primary driver of cellular cytotoxicity. We hypothesize that cancer cells with a high basal burden on their ERAD and UPR pathways are more likely to allow CB-5083 to tip the balance toward irresolvable proteotoxic stress and that elevated basal levels of genes such as DR5 may be indicators of greater susceptibility to proteotoxic stress-induced death. The correlation of MAPK pathway activation and CB-5083 sensitivity was less expected, although it also makes sense that pathways activating protein synthesis would rely more heavily on protein degradation to maintain protein homeostasis. One downstream effect of having an activated MAPK pathway is increased protein synthesis (Dasgupta et al., 2005). Another mechanism that can drive increased protein synthesis is the activation of eIF4E by ERK (Flynn et al., 1997). Given this hypothesis, CB-5083 may be active in a diverse collection of MAPK activation settings, whereas specific targeted agents such as vemurafenib (Bucheit and Davies, 2014) are active only in settings in which the specific target is mutated. Furthermore, CB-5083 may be active as a second line therapy in those patients who become resistant to such targeted agents or even in combination to increase durability of responses.

Given the above, CB-5083 was progressed through pre-clinical development and is currently being evaluated in two phase 1 clinical trials, in patients with relapsed and refractory multiple myeloma and in patients with advanced solid tumors.

EXPERIMENTAL PROCEDURES

Biochemical Assays

WT and mutant p97 proteins were expressed in BL21 (DE3) *E. coli* cells utilizing the pD441-NH vector with a T5 inducible promoter (DNA2.0), as a His-tagged protein and purified by fast protein liquid chromatography (FPLC) His-Trap column chromatography. The hexameric p97 complex was further separated by FPLC S200 size-exclusion chromatography. CB-5083 IC_{50} analyses for p97 and mutants were conducted using a standard NADH-based coupled kinetic ATPase assay and the ADP glo assay (Promega). See the Supplemental Information for assay details.

Cell Assays

TCRα and GFPu cell lines were a kind gift from Ron Kopito (Stanford University). Cancer cell lines were obtained from American Type Culture Collection and cultured according to the supplier's instructions. Immunofluorescence and western blotting assay were conducted using standard procedures. For qPCR assays, RNA was extracted from cell lysates, and cDNA was prepared. Transcript levels were measured by qPCR using a UPR PCR array (SABiosciences) or Taqman primers in the QuantStudio 6 Flex PCR system (Life Technologies). See the Supplemental Information for further assay details.

Animal Studies

The animal research conducted for this study was reviewed and approved by the Institutional Animal Care and Use Committee of Cleave Biosciences. All mice were treated in accordance with guidelines outlined by the Institute for Laboratory Animal Research Guide for the Care and Use of Laboratory Animals. Female athymic nude mice and SCID-Beige mice, 5–8 weeks of age and weighing approximately 20–25 g, were purchased from Charles River Laboratories. Details about animal husbandry can be found in the Supplemental Information. Cancer cell line xenografts were established by implanting 5×10^6 to 10×10^6 cells subcutaneously. CB-5083, MLN9708, and the CB-5083 vehicle (0.5% methyl cellulose in water) were administered by oral gavage and bortezomib and carfilzomib by tail vein injection. Tumor volume and body weights were measured twice weekly and daily, respectively, throughout the study.

ACCESSION NUMBERS

The accession number for the RNA-seq data reported in this paper is GEO: GSE73588.

SUPPLEMENTAL INFORMATION

Supplemental Information includes Supplemental Experimental Procedures, seven figures, and three tables and can be found with this article online at http://dx.doi.org/10.1016/j.ccell.2015.10.002.

AUTHOR CONTRIBUTIONS

Conceptualization, D.J.A., R.L.M, S.D., B.K., F.M.Y., L.S., H.J.Z., D.W., and M.R.; Methodology, D.J.A., R.L.M., S.D., B.K., J.R., S.W., J.W., M.K., and B.T.A.; Investigation, D.J.A., R.L.M, S.D., B.K., J.R., S.W., J.W., B.Y., E.V., S.K.V.S., A.M., F.S., M.K.M., Z.Y.W., M.K., and Y.C.; Resources, B.Y., H.J.Z, D.W.; Writing – Original Draft, D.J.A., R.L.M., S.D., B.K., and M.R.; Writing – Review & Editing, D.J.A, R.L.M., S.D, L.S., H.J.Z., D.W., and M.R.; Supervision, D.J.A, R.L.M., J.S.W., F.M.Y., L.S., H.J.Z., D.W., and M.R.

ACKNOWLEDGMENTS

We thank Alessandra Cesano, Michael Longi, Raymond Deshaies, Ethan Emberley, and Francesco Parlati for scientific discussion and contributions to work presented in this report. We thank L. Gilbert and B. Adamson for discussions regarding the CRISPR studies. M.K. was supported by National Institutes of Health/National Cancer Institute Pathway to Independence Award K99 CA181494. B.T.A. is supported by the Multiple Myeloma Research Foundation and The Stephen & Nancy Grand Multiple Myeloma Translational Initiative.

D.J.A., R.L., S.D., B.K., J.R., S.W., J.W., B.Y., E.V., S.K., A.M., F.S., M-K.M., Z.Y.W., F.M.Y., L.S., H-J.Z., D.W., and M.R. are or were full time employees or full time consultants of Cleave Biosciences.

Received: April 2, 2015
Revised: August 4, 2015
Accepted: October 6, 2015
Published: November 9, 2015

REFERENCES

Barretina, J., Caponigro, G., Stransky, N., Venkatesan, K., Margolin, A.A., Kim, S., Wilson, C.J., Lehár, J., Kryukov, G.V., Sonkin, D., et al. (2012). The Cancer Cell Line Encyclopedia enables predictive modelling of anticancer drug sensitivity. Nature *483*, 603–607.

Bence, N.F., Sampat, R.M., and Kopito, R.R. (2001). Impairment of the ubiquitin-proteasome system by protein aggregation. Science *292*, 1552–1555.

Benjamini, Y., and Yekutieli, D. (2001). The control of the false discovery rate in multiple testing under dependency. Ann. Stat. *29*, 1165–1188.

Bjørkøy, G., Lamark, T., and Johansen, T. (2006). p62/SQSTM1: a missing link between protein aggregates and the autophagy machinery. Autophagy *2*, 138–139.

Bucheit, A.D., and Davies, M.A. (2014). Emerging insights into resistance to BRAF inhibitors in melanoma. Biochem. Pharmacol. *87*, 381–389.

Bug, M., and Meyer, H. (2012). Expanding into new markets—VCP/p97 in endocytosis and autophagy. J. Struct. Biol. *179*, 78–82.

Chou, T.-F., Brown, S.J., Minond, D., Nordin, B.E., Li, K., Jones, A.C., Chase, P., Porubsky, P.R., Stoltz, B.M., Schoenen, F.J., et al. (2011). Reversible inhibitor of p97, DBeQ, impairs both ubiquitin-dependent and autophagic protein clearance pathways. Proc. Natl. Acad. Sci. U S A *108*, 4834–4839.

Chou, T.-F., Li, K., Frankowski, K.J., Schoenen, F.J., and Deshaies, R.J. (2013). Structure-activity relationship study reveals ML240 and ML241 as potent and selective inhibitors of p97 ATPase. ChemMedChem *8*, 297–312.

Cillo, C., Dick, J.E., Ling, V., and Hill, R.P. (1987). Generation of drug-resistant variants in metastatic B16 mouse melanoma cell lines. Cancer Res. *47*, 2604–2608.

Cole, A., Wang, Z., Coyaud, E., Voisin, V., Gronda, M., Jitkova, Y., Mattson, R., Hurren, R., Babovic, S., Maclean, N., et al. (2015). Inhibition of the mitochondrial protease ClpP as a therapeutic strategy for human acute myeloid leukemia. Cancer Cell *27*, 864–876.

Dalal, S., Rosser, M.F., Cyr, D.M., and Hanson, P.I. (2004). Distinct roles for the AAA ATPases NSF and p97 in the secretory pathway. Mol. Biol. Cell *15*, 637–648.

Dasgupta, B., Yi, Y., Chen, D.Y., Weber, J.D., and Gutmann, D.H. (2005). Proteomic analysis reveals hyperactivation of the mammalian target of rapamycin pathway in neurofibromatosis 1-associated human and mouse brain tumors. Cancer Res. *65*, 2755–2760.

DeLaBarre, B., Christianson, J.C., Kopito, R.R., and Brunger, A.T. (2006). Central pore residues mediate the p97/VCP activity required for ERAD. Mol. Cell *22*, 451–462.

Deshaies, R.J. (2014). Proteotoxic crisis, the ubiquitin-proteasome system, and cancer therapy. BMC Biol. *12*, 94.

Fang, C.J., Gui, L., Zhang, X., Moen, D.R., Li, K., Frankowski, K.J., Lin, H.J., Schoenen, F.J., and Chou, T.F. (2015). Evaluating p97 inhibitor analogues for their domain selectivity and potency against the p97-p47 complex. ChemMedChem *10*, 52–56.

Fessart, D., Marza, E., Taouji, S., Delom, F., and Chevet, E. (2013). P97/CDC-48: proteostasis control in tumor cell biology. Cancer Lett. *337*, 26–34.

Flynn, A., Vries, R.G., and Proud, C.G. (1997). Signalling pathways which regulate eIF4E. Biochem. Soc. Trans. *25*, 192S.

Gilbert, L.A., Horlbeck, M.A., Adamson, B., Villalta, J.E., Chen, Y., Whitehead, E.H., Guimaraes, C., Panning, B., Ploegh, H.L., Bassik, M.C., et al. (2014). Genome-scale CRISPR-mediated control of gene repression and activation. Cell *159*, 647–661.

Hideshima, T., Richardson, P., Chauhan, D., Palombella, V.J., Elliott, P.J., Adams, J., and Anderson, K.C. (2001). The proteasome inhibitor PS-341 inhibits growth, induces apoptosis, and overcomes drug resistance in human multiple myeloma cells. Cancer Res. *61*, 3071–3076.

Johnson, D.E. (2015). The ubiquitin-proteasome system: opportunities for therapeutic intervention in solid tumors. Endocr. Relat. Cancer *22*, T1–T17.

Ju, J.S., Fuentealba, R.A., Miller, S.E., Jackson, E., Piwnica-Worms, D., Baloh, R.H., and Weihl, C.C. (2009). Valosin-containing protein (VCP) is required for autophagy and is disrupted in VCP disease. J. Cell Biol. *187*, 875–888.

Kupperman, E., Lee, E.C., Cao, Y., Bannerman, B., Fitzgerald, M., Berger, A., Yu, J., Yang, Y., Hales, P., Bruzzese, F., et al. (2010). Evaluation of the proteasome inhibitor MLN9708 in preclinical models of human cancer. Cancer Res. *70*, 1970–1980.

Lu, M., Lawrence, D.A., Marsters, S., Acosta-Alvear, D., Kimmig, P., Mendez, A.S., Paton, A.W., Paton, J.C., Walter, P., and Ashkenazi, A. (2014). Cell death. Opposing unfolded-protein-response signals converge on death receptor 5 to control apoptosis. Science *345*, 98–101.

Luo, J., Solimini, N.L., and Elledge, S.J. (2009). Principles of cancer therapy: oncogene and non-oncogene addiction. Cell *136*, 823–837.

Magnaghi, P., D'Alessio, R., Valsasina, B., Avanzi, N., Rizzi, S., Asa, D., Gasparri, F., Cozzi, L., Cucchi, U., Orrenius, C., et al. (2013). Covalent and allosteric inhibitors of the ATPase VCP/p97 induce cancer cell death. Nat. Chem. Biol. *9*, 548–556.

Meacham, C.E., and Morrison, S.J. (2013). Tumour heterogeneity and cancer cell plasticity. Nature *501*, 328–337.

Meerang, M., Ritz, D., Paliwal, S., Garajova, Z., Bosshard, M., Mailand, N., Janscak, P., Hübscher, U., Meyer, H., and Ramadan, K. (2011). The ubiquitin-selective segregase VCP/p97 orchestrates the response to DNA double-strand breaks. Nat. Cell Biol. *13*, 1376–1382.

Meyer, H., Bug, M., and Bremer, S. (2012). Emerging functions of the VCP/p97 AAA-ATPase in the ubiquitin system. Nat. Cell Biol. *14*, 117–123.

Milano, A., Perri, F., and Caponigro, F. (2009). The ubiquitin-proteasome system as a molecular target in solid tumors: an update on bortezomib. Onco Targets Ther. *2*, 171–178.

Miura, G. (2014). ER stress: to live or let die. Nat. Chem. Biol. *10*, 695–695.

Morris, J.A., Dorner, A.J., Edwards, C.A., Hendershot, L.M., and Kaufman, R.J. (1997). Immunoglobulin binding protein (BiP) function is required to protect cells from endoplasmic reticulum stress but is not required for the secretion of selective proteins. J. Biol. Chem. *272*, 4327–4334.

Morris, L.L., Hartman, I.Z., Jun, D.J., Seemann, J., and DeBose-Boyd, R.A. (2014). Sequential actions of the AAA-ATPase valosin-containing protein (VCP)/p97 and the proteasome 19 S regulatory particle in sterol-accelerated, endoplasmic reticulum (ER)-associated degradation of 3-hydroxy-3-methylglutaryl-coenzyme A reductase. J. Biol. Chem. *289*, 19053–19066.

Nguyen, T.K., and Grant, S. (2014). Dinaciclib (SCH727965) inhibits the unfolded protein response through a CDK1- and 5-dependent mechanism. Mol. Cancer Ther. *13*, 662–674.

Oda, Y., Okada, T., Yoshida, H., Kaufman, R.J., Nagata, K., and Mori, K. (2006). Derlin-2 and Derlin-3 are regulated by the mammalian unfolded protein response and are required for ER-associated degradation. J. Cell Biol. *172*, 383–393.

Ogata, M., Hino, S., Saito, A., Morikawa, K., Kondo, S., Kanemoto, S., Murakami, T., Taniguchi, M., Tanii, I., Yoshinaga, K., et al. (2006). Autophagy is activated for cell survival after endoplasmic reticulum stress. Mol. Cell. Biol. *26*, 9220–9231.

Oromendia, A.B., and Amon, A. (2014). Aneuploidy: implications for protein homeostasis and disease. Dis. Model. Mech. *7*, 15–20.

Patricelli, M.P., Nomanbhoy, T.K., Wu, J., Brown, H., Zhou, D., Zhang, J., Jagannathan, S., Aban, A., Okerberg, E., Herring, C., et al. (2011). In situ kinase profiling reveals functionally relevant properties of native kinases. Chem. Biol. *18*, 699–710.

Rabinovich, E., Kerem, A., Fröhlich, K.U., Diamant, N., and Bar-Nun, S. (2002). AAA-ATPase p97/Cdc48p, a cytosolic chaperone required for endoplasmic reticulum-associated protein degradation. Mol. Cell. Biol. *22*, 626–634.

Ramos, P., and Bentires-Alj, M. (2014). Mechanism-based cancer therapy: resistance to therapy, therapy for resistance. Oncogene *34*, 3617–3626.

Ruschak, A.M., Slassi, M., Kay, L.E., and Schimmer, A.D. (2011). Novel proteasome inhibitors to overcome bortezomib resistance. J. Natl. Cancer Inst. *103*, 1007–1017.

Sano, R., and Reed, J.C. (2013). ER stress-induced cell death mechanisms. Biochim. Biophys. Acta *1833*, 3460–3470.

Schenone, S., Brullo, C., Musumeci, F., Radi, M., and Botta, M. (2011). ATP-competitive inhibitors of mTOR: an update. Curr. Med. Chem. *18*, 2995–3014.

Song, C., Wang, Q., and Li, C.C. (2003). ATPase activity of p97-valosin-containing protein (VCP). D2 mediates the major enzyme activity, and D1 contributes to the heat-induced activity. J. Biol. Chem. *278*, 3648–3655.

Song, B.L., Sever, N., and DeBose-Boyd, R.A. (2005). Gp78, a membrane-anchored ubiquitin ligase, associates with Insig-1 and couples sterol-regulated ubiquitination to degradation of HMG CoA reductase. Mol. Cell *19*, 829–840.

Teicher, B.A., Ara, G., Herbst, R., Palombella, V.J., and Adams, J. (1999). The proteasome inhibitor PS-341 in cancer therapy. Clin. Cancer Res. *5*, 2638–2645.

Van Drie, J.H. (2011). Protein folding, protein homeostasis, and cancer. Chin. J. Cancer *30*, 124–137.

Wacker, S.A., Houghtaling, B.R., Elemento, O., and Kapoor, T.M. (2012). Using transcriptome sequencing to identify mechanisms of drug action and resistance. Nat. Chem. Biol. *8*, 235–237.

Wang, Y., Serradell, N., Bolos, J., and Rosa, E. (2007). YM-155: apoptosis inducer survivin expression inhibitor oncolytic. Drugs Future *32*, 879–882.

Wang, Q., Mora-Jensen, H., Weniger, M.A., Perez-Galan, P., Wolford, C., Hai, T., Ron, D., Chen, W., Trenkle, W., Wiestner, A., and Ye, Y. (2009). ERAD inhibitors integrate ER stress with an epigenetic mechanism to activate BH3-only protein NOXA in cancer cells. Proc. Natl. Acad. Sci. USA *106*, 2200–2205.

Wang, Q., Shinkre, B.A., Lee, J.G., Weniger, M.A., Liu, Y., Chen, W., Wiestner, A., Trenkle, W.C., and Ye, Y. (2010). The ERAD inhibitor Eeyarestatin I is a bifunctional compound with a membrane-binding domain and a p97/VCP inhibitory group. PLoS ONE *5*, e15479.

Wright, J.J. (2010). Combination therapy of bortezomib with novel targeted agents: an emerging treatment strategy. Clin. Cancer Res. *16*, 4094–4104.

Wustrow, D., Zhou, H.-J., and Rolfe, M. (2013). Inhibition of ubiquitin proteasome system enzymes for anticancer therapy. In Annual Reports in Medicinal Chemistry, C.D. Manoj, ed. (Academic Press), pp. 205–225.

Yamamoto, A., Tagawa, Y., Yoshimori, T., Moriyama, Y., Masaki, R., and Tashiro, Y. (1998). Bafilomycin A1 prevents maturation of autophagic vacuoles by inhibiting fusion between autophagosomes and lysosomes in rat hepatoma cell line, H-4-II-E cells. Cell Struct. Funct. *23*, 33–42.

Ye, Y., Meyer, H.H., and Rapoport, T.A. (2001). The AAA ATPase Cdc48/p97 and its partners transport proteins from the ER into the cytosol. Nature *414*, 652–656.

Yoshida, H., Okada, T., Haze, K., Yanagi, H., Yura, T., Negishi, M., and Mori, K. (2000). ATF6 activated by proteolysis binds in the presence of NF-Y (CBF) directly to the cis-acting element responsible for the mammalian unfolded protein response. Mol. Cell. Biol. *20*, 6755–6767.

Zhang, L., Pham, L.V., Newberry, K.J., Ou, Z., Liang, R., Qian, J., Sun, L., Blonska, M., You, Y., Yang, J., et al. (2013). In vitro and in vivo therapeutic efficacy of carfilzomib in mantle cell lymphoma: targeting the immunoproteasome. Mol. Cancer Ther. *12*, 2494–2504.